Available online at www.sciencedirect.com
ScienceDirect
Journal of Power Sources 179 (2008) 371–380
JOURNAL OF POWER SOURCES
www.elsevier.com/locate/jpowsour

# Characterization of solid electrode materials using chronoamperometry: A study of the alkaline γ-$MnO_2$ electrode

Aaron P. Malloy, Scott W. Donne *

*Discipline of Chemistry, University of Newcastle, Callaghan, NSW 2308, Australia*

Received 30 August 2007; received in revised form 12 October 2007; accepted 14 December 2007
Available online 11 January 2008

**Abstract**

Large voltage step chronoamperometry is shown to be a time-efficient means to examine solid electrode materials compared with conventional electrochemical methods such as linear sweep voltammetry (LSV) and step potential electrochemical spectroscopy (SPECS), all the while providing comparable information concerning the rate capability of a material and its capacity. The applicability of the technique is demonstrated through a study of the alkaline γ-$MnO_2$ electrode. By sampling the current (and hence the charge) at various times after the chronoamperometric voltage step, the compatibility between chronoamperometry and LSV is disclosed. Furthermore, modelling of the chronoamperometric data using two curves based on a spherical diffusion model representing fast and slow discharge processes are found to be statistically suitable. From this modelling, values of $A\sqrt{D}$ (where $A$ is the electrochemically active surface area and $D$ is the diffusion coefficient) for the two processes are $3.89 \times 10^{-4}$ and $0.70 \times 10^{-4}$ $cm^3\ s^{-1/2}\ g^{-1}$, respectively, both of which are comparable with $A\sqrt{D}$ data extracted from a SPECS experiment on an identical electrode.


*Keywords:* Chronoamperometry; Solid electrodes; Solid-state diffusion; Manganese dioxide; Electrochemically active surface area

## 1. Introduction

In modern society there is an increasing trend towards electronic portability (*e.g.*, computers, compact disc players, flashlights), and as such an increasing demand is being placed on the batteries that are used to power these devices. The aqueous alkaline Zn|$MnO_2$ cell is a popular choice as a portable power supply due to the good electrochemical properties of the manganese dioxide cathode. Despite this popularity and performance fundamental understanding of the behaviour of the manganese dioxide is very limited, due mainly to the complex interplay between material structure and electrochemical performance [1–3].

When characterizing the electrochemical behaviour of a commercial solid electrode system it is desirable to gain as much information as possible with a minimum number of experiments so as to save sample quantity and be more efficient time-wise. There are numerous techniques available to the electrochemist to characterize material performance including: (i) potentiodynamic methods such as linear sweep and cyclic voltammetry (LSV and CV, respectively); (ii) potentiostatic methods such as chronoamperometry and the more elaborate method of step potential electrochemical spectroscopy (SPECS); (iii) galvanostatic methods such as chronopotentiometry and the galvanostatic intermittent titration technique (GITT); (iv) techniques based in the frequency domain such as electrochemical impedance spectroscopy (EIS). To extract a complete performance profile of the material being considered, i.e., over the entire discharge compositional range, quite often it is necessary to either combine methods or establish an iterative sequence to achieve this goal. For example, the techniques of LSV/CV and chronopotentiometry are essentially used solely for comparative purposes since the results describe the kinetic performance of a given material only under one set of conditions, i.e., voltage scan rate or current density. The more elaborate SPECS and GITT methods, while providing both thermodynamic and kinetic information,

* Corresponding author. Tel.: +61 2 4921 5477; fax: +61 2 4921 5472.
*E-mail address:* scott.donne@newcastle.edu.au (S.W. Donne).

0378-7753/$ – see front matter © 2008 Elsevier B.V. All rights reserved.
doi:10.1016/j.jpowsour.2007.12.108

are prone to taking extended periods of time to conduct a single experiment, in which case material and system stability becomes an issue. Similarly, a single EIS measurement yields very little information about the system as a whole and so it must be combined with another technique that changes the solid electrode composition in a systematic fashion. In general, with solid electrode systems being essentially single-use only, i.e., past electrode charge–discharge history is important, it is clear that a trade-off has to be made between the amount of useful data extracted versus the time taken to collect that data.

To elaborate further, SPECS is a very common technique that is known to produce considerable thermodynamic and kinetic electrochemical data from a single experiment. A SPECS experiment involves applying a small voltage step (5–25 mV) to the solid electrode that is followed by an extended rest time during which the resultant current is recorded as a function of time [1–10]. When a pre-defined experimental limit has been reached, i.e., minimal current or a fixed time, the voltage is stepped again and the process repeated so that it ultimately covers the usable discharge or charge compositional range. From the resultant current transients, kinetic information such as a diffusion coefficient (as a function of composition) can be extracted provided a satisfactory model is adopted. It is important at this point to be clear that extraction of a diffusion coefficient is only appropriate when dealing with solid-state systems that undergo single-phase (solid solution or homogeneous) reduction. Furthermore, if the rest time is sufficient, quasi-thermodynamic data can also be extracted. While this technique produces a large amount of very useful data, the time required for the process is a major drawback. Depending on the conditions used, a SPECS experiment can take over 2 weeks to complete. This not only makes the technique susceptible to any chemical instability that the electrode might suffer, but also limits the number of experiments that can be conducted and exposes the overall process to external problems such as power interruptions.

In this study, an existing electrochemical technique is adopted to a solid electrode system with the objective of producing sufficient data to characterize material performance within a reasonable timeframe. Instead of applying a sequence of small voltage steps as in a SPECS experiment, the approach has been to apply a much larger voltage step (0.1–0.5 V from the open-circuit voltage (OCV)), and then interpret the resultant data with a suitable chronoamperometric model. This experimental technique is evaluated using the alkaline manganese dioxide ($\gamma$-$MnO_2$) electrode.

## 2. Experimental

### 2.1. Materials

The manganese dioxide was provided by Delta EMD Australia, Pty Limited [11]. It was prepared by anodic electrolysis on to a Ti substrate from a hot (~98 °C) acidic ($H_2SO_4$) solution of $MnSO_4$, in which the $H_2SO_4$:Mn ratio was ~0.4. When sufficient material had been deposited, the Ti anode was removed from the electrolysis cell and the deposit was mechanically stripped from the substrate. The product was subsequently milled to a −105-μm powder, neutralized and washed to remove any remaining electrolyte, and then dried at 110 °C. Materials produced in this fashion are called electrolytic manganese dioxide (EMD). Using standard analytical techniques it was determined that the EMD sample possessed the γ-crystal structure (X-ray diffraction using Cu Kα radiation) [3], had a O:Mn ratio of 1.96 [12], a water content of 1.72 wt.% [13–15], and a BET surface area ($N_2$ adsorption at 77 K) of 32 $m^2\ g^{-1}$ [16].

### 2.2. Electrochemical cell construction [1,2]

The working electrode blackmix was prepared by lightly grinding together in a mortar and pestle the EMD (0.45 g), Timcal SFG6 graphite (4.5 g) and 9 M (37%) KOH (1.105 g). After ~5 min of mixing, the blackmix was stored in an airtight container for 24 h to allow equilibration to occur, i.e., the electrolyte to fully wet the EMD surface.

The electrochemical cell is shown schematically in Fig. 1. An amount of working electrode blackmix corresponding to 0.015 g of EMD was placed in a Teflon-lined gold-coated C-size battery can. The inner surface of the Teflon was brushed down to remove attached particles and three layers of separator paper were laid on top of the sample. The mixture was then compressed under 1 t for 60 s to form a compact electrode that was in good contact with the can base. After compression, a perforated Perspex separator disc was added, followed by a stainless-steel counter electrode. The chamber was then filled with ~15 mL of 9 M KOH electrolyte and a Perspex cap was inserted into the top. The cell was mounted on top of a brass current-collector between a Perspex cover and base plate, and secured in place by three bolts that were tightened to a common torque of 0.75 cNm to ensure uniform pressure. To complete the cell, a Hg|HgO reference electrode (9 M KOH) was inserted through the Perspex cap.

### 2.3. Discharge protocol

To determine the starting potential, the OCV of the EMD was determined. Sufficient EMD to form a thin layer on the

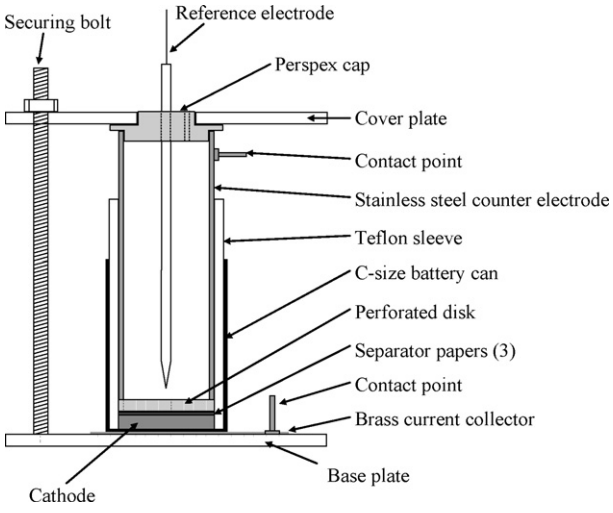


Fig. 1. Schematic of electrochemical cell.

bottom of a plastic sample vial (50-mL volume) was covered with ~20 mL of 9 M KOH solution, shaken and allowed to settle and equilibrate in a sealed environment for 24 h. The OCV was measured by placing a Pt disc electrode into contact with the EMD in the vial and measuring its potential with respect to a Hg|HgO reference electrode in the same solution.

Identical individual cells were prepared from the above-mentioned composite working electrode mixture for the chronoamperometry experiments. This was not intended to reflect the proposed electrochemical technique, but rather attempts to understand the behaviour of the alkaline EMD electrode under such conditions. Each cell was then charged to the OCV (0.261 V), at which it was then held for a 1-h rest period. The last-mentioned step was necessary because, in an alkaline environment, EMD is chemically reduced by the surface functional groups on the graphite. After this rest period, the potential was stepped cathodically to a predetermined voltage where it was allowed to sit for 7 h with the resulting current recorded as a function of time. The step voltages employed were 0.1, 0.0, −0.1, −0.2, −0.3 and −0.4 V versus Hg|HgO.

For the purposes of comparison, LSV and SPECS experiments were carried out on electrodes constructed in the same fashion. LSV was conducted from the OCV of the material to −0.75 V using a scan rate of either 0.02 or 0.05 mV $s^{-1}$. The protocol used for the SPECS experiment involved sequential 10 mV cathodic steps with a 2 h rest time between steps.

## 3. Results and discussion

### 3.1. Chronoamperometry on alkaline manganese dioxide electrode

The chronoamperometric response of the manganese dioxide electrode to various step voltages is shown in Fig. 2(a). As expected, a greater current resulted when the voltage was stepped to more negative values. From the *i–t* transient, it is quite straightforward to convert this data into chronocoulometric– and hence compositional–data as shown in Fig. 2(b). Again, as expected, discharge of the electrode was greater when the voltage was stepped to lower values.

Before developing a model to extract quantitative information from the chronoamperometric data, considerable qualitative analysis can be carried out since an *i–V–t* relationship has been established. To be able to compare the chronoamperometric data to linear sweep voltammetry, the current at various times after the voltage step was sampled. By doing this for all of the voltage steps, a pseudo-voltammogram can be generated from the chronoamperometry data that effectively shows voltammetric discharge at different rates. Such data are given in Fig. 3, and is compared with LSV experiments at two different rates. Interestingly, there are apparent similarities in the appearance of the *i–V* curves irrespective of how the data were collected. Another notable feature between the different data sets was the time taken to achieve comparable data. In Fig. 3(b), for instance, it appears that the 0.02 mV $s^{-1}$

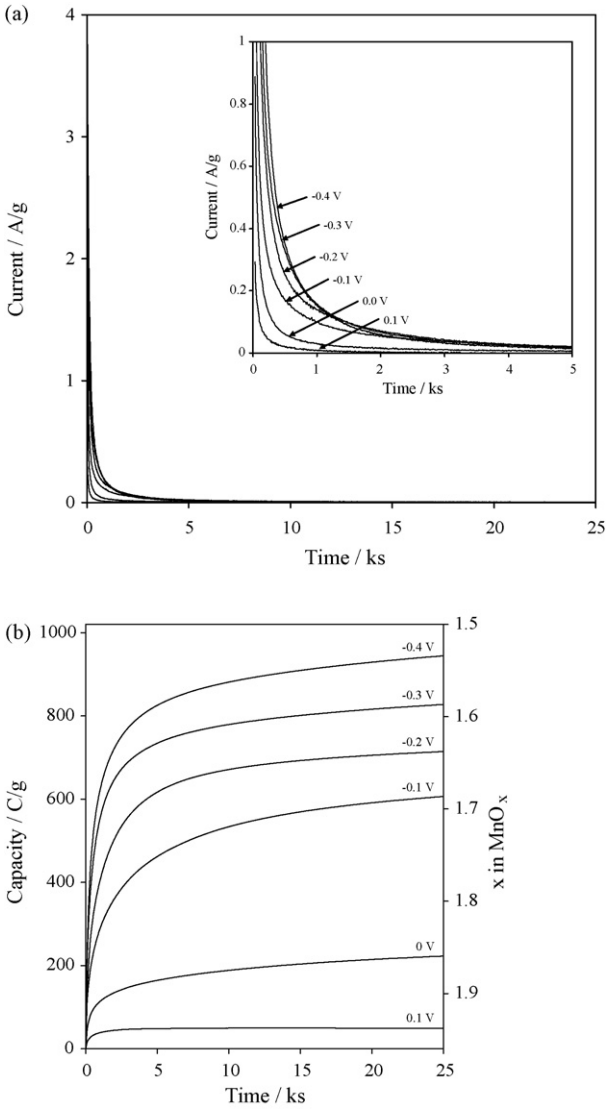


Fig. 2. (a) Chronoamperometric response of alkaline EMD electrode; (b) corresponding chronocoulometric and compositional data.

voltammogram has a similar current response to the chronoamperometric data sampled 2000 s after the voltage step. This is interesting given that it took over 9 h ($33 \times 10^3$ s) to generate this voltammetric data. The similarity in current response is most likely explained simply by the differences in the techniques used, but it does also suggest that equivalent performance data can be obtained in a much shorter timeframe with the used of multiple identical cells and chronoamperometry.

In a similar fashion, the integrated form of the chronoamperometric data (capacity, *Q*) can be compared with capacity data calculated from the LSV experiments, as shown in Fig. 4. Again, the similarities between the data sets are apparent. Now, however, the LSV data is comparable with longer times after the voltage step was made in the chronoamperometric experiments, i.e., 10–20 × $10^3$ s. This is again logical since the capacity extracted from the electrode under these discharges at relatively low rates is expected to at least approach the theoretical

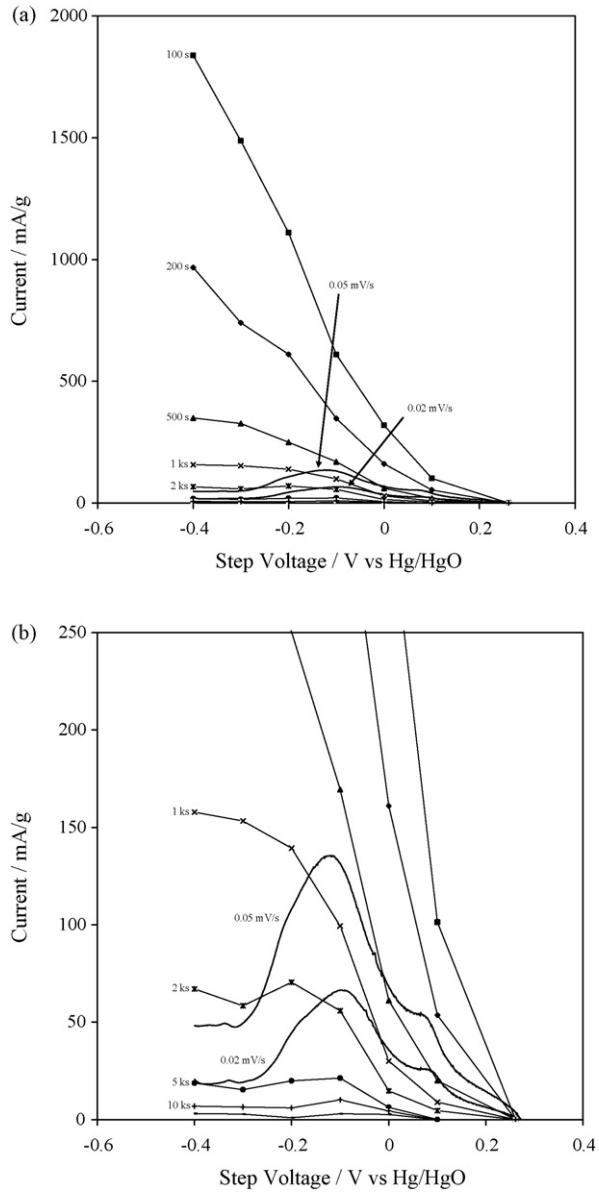


Fig. 3. Comparison between collected chronoamperometric data and corresponding LSV data: (a) original view; (b) expanded view.

capacity limit (1109 C $g^{-1}$), which with chronoamperometry experiments can only be extracted after long periods of time at low voltages.

The performance of a battery electrode material can be evaluated in part by its rate capability and capacity, which from a strictly performance perspective are the two important characteristics. From the above initial analysis, it would seem that large voltage step chronoamperometry is a valuable technique for characterizing both of these electrode characteristics. Voltammetric data are related to chronoamperometric data in Fig. 3 and certainly from a rate capability perspective, the greater current flowing at short times after the voltage step, the better is the rate capability. With large voltage step chronoamperometry the total capacity is also easily extracted, here after extended times at the step voltage.

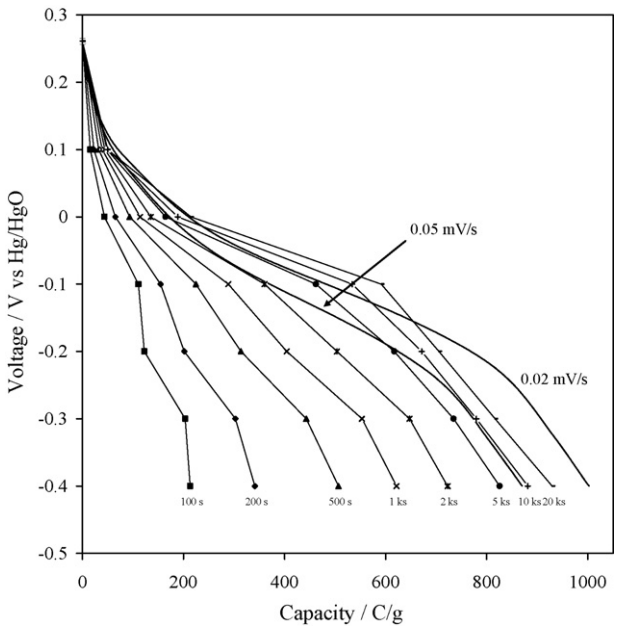


Fig. 4. Comparison between capacity data extracted from LSV (0.02 and 0.05 mV $s^{-1}$) and chronoamperometry.

### 3.2. Discharge mechanism of alkaline manganese dioxide electrode

To begin to model the chronoamperometry data, it is first necessary to elaborate upon the discharge mechanism that the EMD electrode undergoes in an alkaline electrolyte. Many authors have studied the discharge of the alkaline manganese dioxide electrode [17–30]. The basis of our current understanding was proposed initially by Kozawa et al. [31–35] who described a two-step mechanism. In the first step (electron–proton mechanism), an electron from the external circuit is inserted into the manganese dioxide structure to reduce an $Mn^{4+}$ ion to $Mn^{3+}$. To maintain structural charge balance, a water molecule present at the manganese dioxide|electrolyte interface dissociates into a proton, which is inserted into the structure, and an $OH^-$ ion that remains in the electrolyte. This step in the overall mechanism is a homogeneous process that leads to the formation of a solid solution of hydrogen in the host manganese dioxide structure, i.e.,

$$MnO_2 + \Delta H_2O + \Delta e^- \rightarrow MnOOH_\Delta + \Delta OH^- \quad (1)$$

where $\Delta$ is the mole fraction of hydrogen inserted into the structure ($0 < \Delta < 1$). Inserted protons diffuse into the bulk of the structure by hopping to adjacent sites until, ultimately, the hydrogen is distributed uniformly throughout the host structure. This one-electron reaction is primarily responsible for the power that can be extracted from the alkaline manganese dioxide electrode. Subsequent refinements to this step in the mechanism include the introduction of structural features in the original manganese dioxide such as cation vacancies (□), $Mn^{3+}$ ions and structural

water [13–15], i.e.,

$$(Mn^{4+})_{1-x-y}(\square)_x(Mn^{3+})_y(O^{2-})_{2-4x-y}(OH^-)_{4x+y} + \Delta H_2O + \Delta e^- \rightarrow (Mn^{4+})_{1-x-y-\Delta}(\square)_x(Mn^{3+})_{y+\Delta}(O^{2-})_{2-4x-y-\Delta}(OH^-)_{4x+y+\Delta} + \Delta OH^- \quad (2)$$

where $x$ and $y$ are the mole fractions of cation vacancies and $Mn^{3+}$ ions, respectively. It should be noted that protons (structural water) are used to compensate for charge discrepancies in the structure. A later refinement was the identification of structurally (and hence energetically) different domains within the manganese dioxide structure, which are hence reduced at different voltages [3,5–10,17–23]. These different domains are present in the structure of the manganese dioxide produced by electrolysis, namely γ-$MnO_2$. This polymorph of manganese dioxide has been described in simple terms as a microscopic intergrowth between the pyrolusite (β-$MnO_2$) and the ramsdellite forms of manganese dioxide [36], as shown in Fig. 5. Despite this apparent simplicity, the structure is complicated by the cation vacancies, $Mn^{3+}$ ions and structural water mentioned previously, and indicated in Fig. 5, as well as by a very finely divided morphology, which makes structural analysis difficult. Additionally, micro-twinning of the γ-$MnO_2$ structure has been postulated to account for various features of its X-ray diffraction pattern, although the actual physical presence of this feature has still to be confirmed [3,37].

The second step in the reduction process, as first described by Kozawa and Jeager [35] and refined by others subsequently [17–19,38–39], involves a dissolution–precipitation mechanism. Here, the first-electron reduction product (MnOOH) undergoes dissolution in the concentrated alkaline electrolyte to form a soluble Mn(III) species. It has been shown [40,41] that this mechanism is relevant only for more concentrated alkaline electrolytes where the solubility of MnOOH is substantial. Once in solution, and at sufficiently low voltages, the Mn(III) species undergoes reduction at a conductive surface within the cathode to form a soluble Mn(II) species, which precipitates as $Mn(OH)_2$ almost immediately. Given that $Mn(OH)_2$ is a poor conductor, this causes passivation throughout the electrode. Overall, the second step in the mechanism occurs at too low a voltage to be useful, and also has poor efficiency as a result of the resistive $Mn(OH)_2$ [17–19].

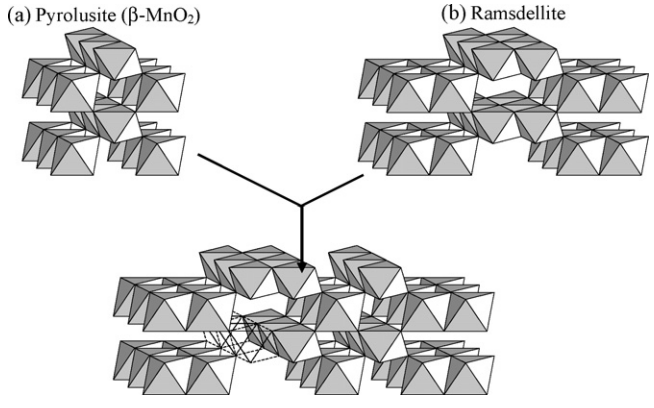


Fig. 5. Microscopic intergrowth of (a) pyrolusite (β-$MnO_2$) and (b) ramsdellite from γ-$MnO_2$.

### 3.3. Development of chronoamperometry model

One of the most common models used to interpret chronoamperometry data is the Cottrell equation [42], i.e.,

$$i(t) = i_d(t) = \frac{nFAD^{1/2}C^*}{\pi^{1/2}t^{1/2}} \quad (3)$$

where $i(t)$ is the current flowing as a function of time $t$ (the subscript d indicates diffusion-limited conditions); $n$ is the stoichiometric number of electrons involved in the redox reaction; $F$ is the Faraday constant; $A$ is the electrochemically active area; $D$ is the active species diffusion coefficient; $C^*$ is the bulk concentration of active species. The Cottrell equation was derived based on semi-infinite planar diffusion, and assuming that the voltage step was sufficiently large so that the surface concentration of active species is essentially zero. From Eq. (3), a plot of $i(t)$ versus $t^{-1/2}$ should give a straight line from which the diffusion coefficient can be extracted. Fig. 6(a) is such a plot for the chronoamperometry data collected in this work. Clearly these plots are not linear, for which a number of possible explanations may be given. The first and most obvious explanation is that the boundary conditions used to derive Eq. (3) do not accurately represent the physical processes occurring in the electrode. This is particularly true since a solid-state electrode is being used in which diffusion is an internal process within each particle, rather than into the bulk of the electrolyte. With a mean particle size of ∼45 μm, this means that the semi-infinite condition will be unsuitable not long after the voltage step because of intersecting diffusion fronts from opposite sides of the particle. Furthermore, the assumption that planar diffusion is apparent is also unreasonable given the morphology of the particles, which is very irregular on both the macroscopic and microscopic scale. Both of these features are also complicated quite considerably by material porosity, which increases the active surface area by at least two orders of magnitude compared with the geometric area based on particle size. Finally, the crystal structure of the active material also plays a part in determining the chronoamperometric response. As described above, and shown in Fig. 5, the structure of γ-$MnO_2$ contains energetically different domains which, for the purposes of these experiments, means that they are reduced at different rates, i.e., different diffusion coefficients. In summary, there may be overlapping processes apparent in the chronoamperometric data, the sum total of which causes deviation from the behaviour predicted by Eq. (3).

To demonstrate this using the Cottrell equation, we can calculate for each of the voltage steps the value $it^{1/2}$, which essentially represents the collection of constants for a particular reduction process. Such data is shown in Fig. 6(b) in comparison with electrode composition. Clearly $it^{1/2}$ (for the most part) decreases over the entire composition range. It is concluded that this indicates, at least within the bounds of the present simple model, that either (or both) $A$ and $D$ decreases with composition, since $C^*$ should increase with an increasing step voltage. The only variation is for the step to the lowest voltage (−0.4 V) where the influence

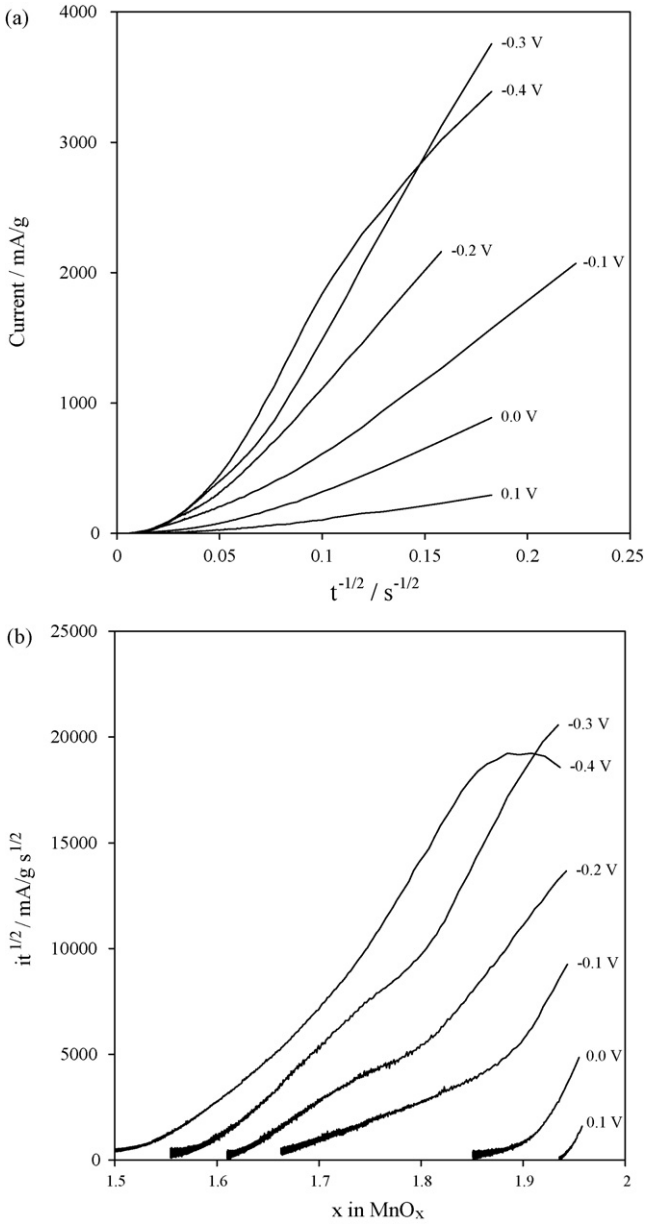


Fig. 6. (a) Chronoamperometry data analysis based on Cottrell equation ($i$–$t^{-1/2}$) and (b) $it^{1/2}$ as a function of composition.

of the second electron reduction is apparent. A decrease in $A$ can be explained by the structural expansion that occurs upon reduction [43]. With the γ-$MnO_2$ being microporous, any swelling due to the inclusion of the larger $Mn^{3+}$ ions into the structure may cause the micropores to close down and thereby limit the active surface area of the electrode material. Similarly, the drop in $D$ can be justified by considering the proton transport mechanism associated with γ-$MnO_2$, since this is believed to be the rate-limiting phenomena [20]. Proton transport occurs via hopping, and is therefore dependent on the availability of unoccupied sites in the direction of diffusion. With a more reduced material, the number of unoccupied sites decreases, essentially inhibiting the rate of proton transport.

A much more advanced diffusion model was developed by Hong et al. [22], albeit for small potential step experiments, but

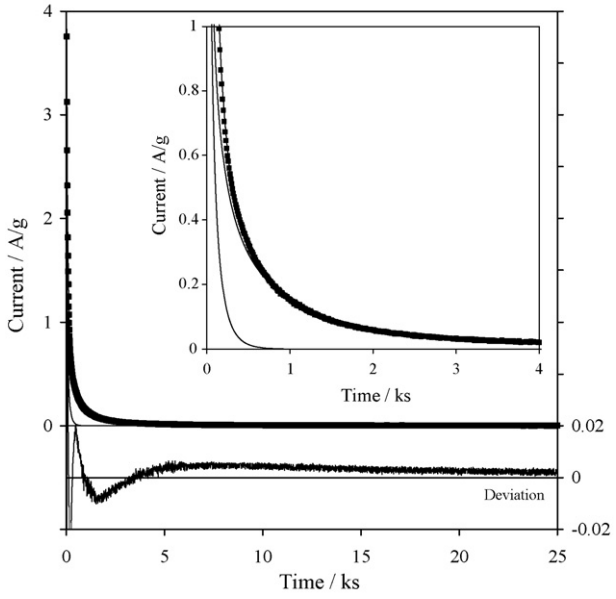


Fig. 7. Comparison between experimental and modelled data based on spherical diffusion into a solid electrode.

adapted here to consider large voltage steps. This model is based on spherical diffusion into a solid electrode material using the following initial and boundary conditions:

$$\text{Initial} : C(x,t) = C_0, \text{ for all } x \text{ when } t = 0 \tag{4}$$

$$\text{Boundary} : C(x,t) = C_1, \text{for } x = 0 \text{ when } t > 0 \tag{5}$$

$$\text{Boundary} : \frac{\partial C(x,t)}{\partial x} = \frac{i(t)}{nFAD}, \text{for } x = 0 \text{ and } a \text{ when } t > 0 \tag{6}$$

Solution of Fick's second law of diffusion under such conditions leads to:

$$i = \frac{2FAD\Delta C}{a}\sum_{n=1}^{\infty} - \frac{n^2\pi^2 Dt}{a^2} \tag{7}$$

where most symbols have already been defined, except for $\Delta C$ which is the change in concentration of hydrogen in the manganese oxide structure over the potential step ($C_1 - C_0$), and $a$ is the radius of the particle. By combining constants in Eq. (7) the fitting parameters $P_1$ and $P_2$ can be produced, i.e.,

$$i = P_1\sum_{n=1}^{\infty}\exp(-n^2 P_2 t) \tag{8}$$

where

$$P_1 = \frac{2FAD\,\Delta C}{a} \tag{9}$$

and

$$P_2 = \frac{\pi^2 D}{a^2} \tag{10}$$

$P_1$ and $P_2$ can now be determined using linear least-squares regression by fitting curve(s) defined by Eq. (7) to the experimen-

tal data. The comparison between the predicted and experimental chronoamperometric data is shown in Fig. 7, where an attempted is also made to address the need for multiple curves defined by Eqs. (7) and (8) to account for the reduction of energetically different sites within the γ-$MnO_2$ electrode. The experimental data used in this figure are for the step to −0.3 V. Fitting two curves leads to a result that quite closely matches the experimental data (average deviation of $\pm 0.004\ A\ g^{-1}$). A similar deviation is apparent for all other data sets that represent steps to other voltages. Fitting a greater number of curves (>2) to the experimental data does not improve the quality of the fit significantly (statistically, *F*-test) enough to warrant their inclusion, despite the already demonstrated presence of more than two processes [1,2]. For two fitted curves, the greatest deviation between the fitted and experimental data occurs at times less than $\sim 2 \times 10^3$ s, which represents the transition from high-rate discharge to a more sustained low-rate extraction of charge. While this definition is somewhat arbitrary, it does perhaps represent complete utilization of certain domains within the structure, while others are continuing to be reduced at a much slower rate. This is also reflected in the inset data in Fig. 7 where there is a very fast process in parallel with a much slower discharge process. It is also apparent that this transition is the greatest source of error in the modelling. $P_1$ and $P_2$ for each of the two processes are shown in Table 1 as a function of the step voltage.

$P_1$ and $P_2$ can also be used to calculate $A\sqrt{D}$ for each process, as shown in Eq. (11):

$$A\sqrt{D} = \frac{\pi}{2F\Delta C}\sqrt{\frac{{P_1}^2}{P_2}} \tag{11}$$

This expression is derived by eliminating the particle radius ($a$) from Eqs. (9) and (10), such that its value does not need to be known. The significance of $A\sqrt{D}$ is that it is an ideal summation for the kinetics of an individual discharge process, since it avoids the need to assume a value for the electrochemically active surface area, which for porous electrode materials is not known with a great degree of certainty. As mentioned above, $\Delta C$ is the change in hydrogen concentration in the manganese structure during discharge. For each process apparent in the chronoamperometric discharge, the first step in determining $\Delta C$ is to calculate the total charge passed as a result of the voltage step. From the X-ray diffraction pattern for the material (Fig. 8), it is then possible to determine the unit-cell dimensions of the γ-$MnO_2$ assuming orthorhombic symmetry [3] and four formula units per unit cell [44]. The charge passed and unit-cell dimensions then allow determination of the average number of hydrogen atoms per unit volume (concentration), and hence the change that occurs with the voltage step. The assumptions made with this calculation are that γ-$MnO_2$ can indeed be described by an orthorhombic unit cell (given the tetragonal nature of β-$MnO_2$ which is a structural component), and that the unit-cell volume remains constant with depth-of-discharge. It is recognized that this last assumption is not strictly true since there have been a number of previous reports that indicate the structure swells on discharge due to the inclusion of protons and Mn(III) in the structure [43]. The expansion is at most 18% based on a comparison of the unit-cell dimensions of ramsdellite ($MnO_2$) and groutite (α-MnOOH) as reported in the literature [44]. While this expansion is significant, the actual relationship between unit-cell volume and depth-of-discharge is not linear, given the structural complexities of the material. Hence, this is the best estimate at this time.

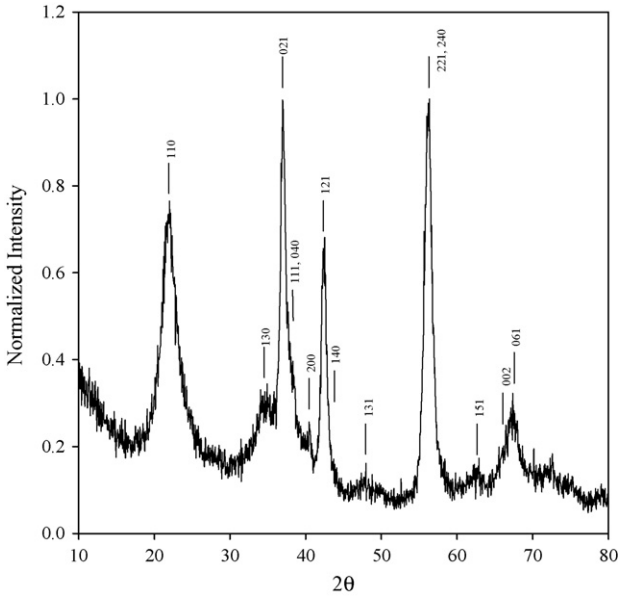


Fig. 8. X-ray diffraction pattern of EMD together with peak assignments based on orthorhombic unit cell.

An important point to mention at this stage is that $A\sqrt{D}$ cannot be separated into individual $A$ and $D$ values because the electrochemically active surface area for manganese dioxide is not known with certainty. The reason for this is due to

Table 1
Data extracted from modelling chronoamperometry data

| Step voltage | Process 1 | | | | Process 2 | | | |
|---|---|---|---|---|---|---|---|---|
| | $P_1$ | $P_2$ | $Q_1$ (C g$^{-1}$) | $A\sqrt{D}$ ($\times 10^{10}$ m$^3$ s$^{-1/2}$ g$^{-1}$) | $P_1$ | $P_2$ | $Q_2$ (C g$^{-1}$) | $A\sqrt{D}$($\times 10^{10}$ m$^3$ s$^{-1/2}$ g$^{-1}$) |
| 0.1 | 0.141 | 6577 | 18 | 4.92 | 0.022 | 469 | 45 | 1.17 |
| 0.0 | 0.402 | 3897 | 92 | 3.64 | 0.011 | 59 | 170 | 0.42 |
| −0.1 | 0.668 | 6212 | 93 | 4.76 | 0.050 | 89 | 544 | 0.51 |
| −0.2 | 0.826 | 3720 | 198 | 3.56 | 0.107 | 161 | 644 | 0.68 |
| −0.3 | 1.607 | 5639 | 247 | 4.48 | 0.237 | 326 | 702 | 0.97 |
| −0.4 | 0.880 | 1276 | 645 | 2.00 | 0.035 | 74 | 460 | 0.46 |

the discrepancy that exists between the methods that are used to measure surface area and the species that are electrochemically active when manganese dioxide is immersed in an alkaline electrolyte. The most common method for surface area measurement is $N_2$ gas adsorption at 77 K, which is subsequently interpreted using the BET isotherm [16]. Typical BET surface areas for commercial EMD lie in the range of 28–32 $m^2\,g^{-1}$, although EMD samples have been produced with BET surface areas that range from 10 to 100 $m^2\,g^{-1}$. Overall, these values indicate that EMD is a very porous material and that in actual fact the surface area is mostly associated with micropores [45]. Compare this method of analysis with the alkaline manganese dioxide electrode interface in which the $H_2O$ molecule is the important adsorbate. Clearly there are significant differences in molecular size, shape, polarity, *etc*., that really limit the applicability of $N_2$ adsorption as a characterization method. Despite the apparent differences in adsorbates, we also need to differentiate between surface area and pore size. As mentioned above, EMD is a microporous material, and on this scale understanding the mass transport of water into and out of the EMD pores is also critical. Because water is consumed in the electrochemical reaction to form $OH^-$ ions, water must diffuse from the bulk solution into the pore to replenish the amount that is consumed, and at the same time $OH^-$ ions must diffuse out of the pore to prevent surface passivation. Therefore, the rate of electrochemical discharge will determine the active surface area since mass transport of electroactive species within material pores exerts an effect.

The calculated values of $A\sqrt{D}$ for each of the two processes are also shown in Table 1 as a function of step voltage. Clearly, Process 1 is kinetically faster (~4 times) than Process 2. This calculation, coupled with the much smaller capacity associated with Process 1 (for the most part), indicates that it represents a structural domain that is readily consumed at a fast rate. The origin of this domain is not known with certainty, but it may be related to reduction of Mn(IV) ions near defects such as cation vacancies in the structure. Furthermore, our previous work [2] has shown that reduction of pyrolusite domains within the structure is also a kinetically fast process. With regards to material design, this represents a desired domain within the γ-$MnO_2$ structure for high-rate performance materials. Process 2, on the other hand, may represent the slightly slower reduction of the majority ramsdellite domains within the structure. Overall, the values obtained here are consistent with those reported previously for studies on γ-$MnO_2$. Many attempts have been documented in the literature concerning the determination of proton diffusion coefficient in γ-$MnO_2$. A wide range of values have been reported ($10^{-11}$–$10^{-18}$ $cm^2\,s^{-1}$) based on measurements made using a variety of methods [46]. If these measurements of $D$ are combined with the area assumed in the calculation, then $A\sqrt{D}$ irrespective of the method can be calculated to be within an order of magnitude of ~$10^{-3}$ $cm^3\,s^{-1/2}\,g^{-1}$. The work reported here is consistent with this; it gives an average value of $3.89 \times 10^{-4}$ $cm^3\,s^{-1/2}\,g^{-1}$ for Process 1 and $0.70 \times 10^{-4}$ $cm^3\,s^{-1/2}\,g^{-1}$ for Process 2. Aside from taking an average value for $A\sqrt{D}$, there does not appear to be any significant trends in the data with step voltage, which is expected given that the same processes are being examined throughout the discharge irrespective of the step voltage.

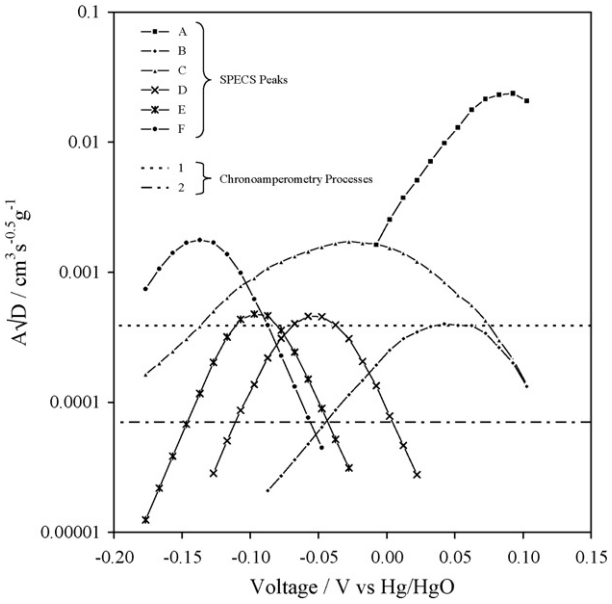


Fig. 9. Comparison between $A\sqrt{D}$ measured using SPECS and large voltage step chronoamperometry.

The value of the large voltage step chronoamperometry experiments becomes apparent when the resultant data are compared with a SPECS experiment on the same electrode. In this case, a 10-mV cathode step was applied every 2 h from the open-circuit voltage to less than −0.4 V. A similar approach was used to model the *i*–*t* transients, i.e., the spherical model described by Eq. (7) combined with the subsequent analysis to determine $A\sqrt{D}$ (Eq. (11)), taking into proportionate account the multiple processes occurring at different voltages (as described in Ref. [2]), and the fact that only a small cathodic voltage step was used. The resultant $A\sqrt{D}$ data is shown in Fig. 9 as a function of electrode voltage (and hence composition), where it is compared with the results obtained using large voltage step chronoamperometry. For the SPECS data, peaks *A*–*F* refer to the component processes that were extracted in the SPECS experiment from the overall γ-$MnO_2$ discharge process. There is a good comparison between the $A\sqrt{D}$ values obtained using the different methods, thus establishing the validity and applicability of our large voltage step chronoamperometry method. As mentioned before, Process 1 reflects the higher discharge rate processes, while Process 2 represents the more sustain, longer lasting extraction of charge.

## 4. Summary and conclusions

The applicability of large voltage step chronoamperometry to the study of solid electrodes has been evaluated, with the alkaline γ-$MnO_2$ electrode representing a test case. The results obtained are compared with those of more conventional LSV and SPECS analysis methods. The motivation of the work is to develop an alternative electrochemical characterization method that is quicker but still provides valuable information. While steps to

multiple voltages are time-consuming experiments when combined they provide the ability to evaluate the method. Routine analysis using this method is to only one step, voltage, namely −0.3 V, so as to examine almost all of the one-electron discharge and avoid complications associated with accessing reduction with the second electron.

From an initial qualitative analysis, it has proved possible to demonstrate similarities between the chronoamperometry and LSV performance data. In particular, by sampling the current at defined times after the voltage step, data have been generated that are comparable with the raw and integrated LSV data (Figs. 3 and 4, respectively).

The chronoamperometry data are then modelled using Fick's second law and assuming spherical diffusion into solid particles. Multiple curves (2) are necessary to match the experimental data, with two curves that statistically represent fast and slow processes. From this analysis values for $A\sqrt{D}$ are extracted ($3.89 \times 10^{-4}\,\mathrm{cm^3\,s^{-1/2}\,g^{-1}}$ for Process 1 and $0.70 \times 10^{-4}\,\mathrm{cm^3\,s^{-1/2}\,g^{-1}}$ for Process 2) are found to match quite closely those reported previously determined by SPECS using the much more time-consuming and complex SPECS technique (Fig. 9).

In conclusion, the effectiveness of large voltage step chronoamperometry as an efficient method for characterizing solid electrode materials has been demonstrated.

## Acknowledgements

The authors acknowledge the financial and technical inputs into this work by Rodney Williams and Andrew Manditch from Delta EMD Australia Pty Limited. Furthermore, the Australian Research Council is acknowledged for their financial support through their Linkage Project scheme (LP0346943).

## References

[1] G.J. Browning, S.W. Donne, J. Appl. Electrochem. 35 (2005) 437.
[2] G.J. Browning, S.W. Donne, J. Appl. Electrochem. 35 (2005) 871.
[3] Y. Chabre, J. Pannetier, Prog. Solid State Chem. 23 (1995) 1.
[4] Y. Chabre, J. Electrochem. Soc. 138 (1991) 329.
[5] W. Bowden, K. Brandt, J.J. Cervera, H.S. Choe, R.A. Sirotina J. Sunstrom, US Patent 6,440,181 (2002).
[6] W. Bowden, R.A. Sirotina, S. Hackney, ITE Lett. 1 (6) (2000) B27.
[7] W. Bowden, C.P. Grey, S. Hackney, X.Q. Yang, Y. Paik, F. Wang, T. Richards, R. Sirotina, ITE Lett. 3 (3) (2002) B1.
[8] W. Bowden, C.P. Grey, R. Sirotina, T. Richards, F. Wang, Y. Paik, ITE Lett. 4 (2) (2003) B1.
[9] W. Bowden, S. Hackney, R. Sirotina, ITE Lett. 4 (1) (2003) B1.
[10] Y. Paik, W. Bowden, T. Richards, R. Sirotina, C.P. Grey, J. Electrochem. Soc. 151 (2004) A998.
[11] C.B. Ward, A.I. Walker, A.R. Taylor, Prog. Batt. Batt. Mater. 11 (1992) 40.
[12] K.J. Vetter, N. Jaeger, Electrochim. Acta 11 (1966) 401.
[13] P. Ruetschi, J. Electrochem. Soc. 131 (1984) 2737.
[14] P. Ruetschi, J. Electrochem. Soc. 135 (1988) 2657.
[15] P. Ruetschi, R. Giovanoli, J. Electrochem. Soc. 135 (1988) 2663.
[16] S. Brunauer, P.H. Emmett, E. Teller, J. Am. Chem. Soc. 60 (1938) 309.
[17] S.W. Donne, G.A. Lawrance, D.A.J. Swinkels, J. Electrochem. Soc. 144 (1997) 2949.
[18] S.W. Donne, G.A. Lawrance, D.A.J. Swinkels, J. Electrochem. Soc. 144 (1997) 2954.
[19] S.W. Donne, G.A. Lawrance, D.A.J. Swinkels, J. Electrochem. Soc. 144 (1997) 2961.
[20] X. Xi, L. Hong, C. Zhenhai, J. Electrochem. Soc. 136 (1989) 266.
[21] D.A.J. Swinkels, K.E. Anthony, P.M. Fredericks, P.R. Osborn, J. Electroanal. Chem. 168 (1984) 433.
[22] Z. Hong, C. Zhenhai, X. Xi, J. Electrochem. Soc. 136 (1989) 2771.
[23] W. Bowden, K. Brandt, J.J. Cervera, H.S. Choe, R.A. Sirotina J. Sunstrom, US Patent 6,509,117 (2003).
[24] J.P. Gabano, J. Seguret, J.F. Laurent, J. Electrochem. Soc. 117 (1970) 147.
[25] A.B. Scott, J. Electrochem. Soc. 107 (1960) 941.
[26] H. Laig-Hörstebrock, J. Electroanal. Chem. 180 (1984) 599.
[27] S. Atlung, T. Jacobsen, Electrochim. Acta 21 (1976) 575.
[28] M.A. Malati, M.W. Rophael, I.I. Bhayat, Electrochim. Acta 26 (1981) 239.
[29] M.W. Rophael, M.A. Malati, Atomkernenergie 25 (1975) 231.
[30] H. Kahil, F. Dalard, J. Guitton, J.P. Cohen-Addad, Surf. Technol. 16 (1982) 331.
[31] A. Kozawa, J.F. Yeager, J. Electrochem. Soc. 112 (1965) 959.
[32] A. Kozawa, R.A. Powers, J. Electrochem. Soc. 113 (1966) 870.
[33] A. Kozawa, R.A. Powers, Electrochem. Technol. 5 (1967) 535.
[34] A. Kozawa, R.A. Powers, J. Electrochem. Soc. 115 (1968) 122.
[35] A. Kozawa, J.F. Jeager, J. Electrochem. Soc. 115 (1968) 1003.
[36] P.M. De Wolff, Acta Cryst. 12 (1959) 341.
[37] A.H. Heuer, A.Q. He, P.J. Hughes, F.H. Feddrix, ITE Lett. Batt., New Tech. Med. 1 (2000) 926.
[38] Y.F. Yao, N. Gupta, H.S. Wroblowa, J. Electroanal. Interf. Electrochem. 223 (1987) 107.
[39] H.S. Wroblowa, N. Gupta, J. Electroanal. Interf. Electrochem. 238 (1987) 93.
[40] (a) D. Qu, L. Bai, C.G. Castledine, B.E. Conway, W.A. Adams, J. Electroanal. Chem. 365 (1994) 247;
(b) D. Qu, B.E. Conway, L. Bai, Z.H. Zhou, W.A. Adams, J. Appl. Electrochem. 23 (1993) 693.
[41] A. Kozawa, T. Kalnoki-Kis, J.F. Yeager, J. Electrochem. Soc. 113 (1966) 405.
[42] A.J. Bard, L.R. Faulkner, Electrochemical Methods: Fundamentals and Applications, John Wiley and Sons, New York, 1980.
[43] J. Fitzpatrick, F.L. Tye, J. Appl. Electrochem. 21 (1991) 130.
[44] (a) R.G. Burns, V.M. Burns, in: A. Kozawa, R.J. Brodd (Eds.), Proceedings of the Manganese Dioxide Symposium, vol. 1, Cleveland, 1975, p. 306;
(b) R.G. Burns, V.M. Burns, in: B. Schumm, H.M. Joseph, A. Kozawa (Eds.), Proceedings of the Manganese Dioxide Symposium, vol. 2, Tokyo, 1980, p. 97.
[45] J.B. Arnott, R.P. Williams, A.G. Pandolfo, S.W. Donne, J. Power Sources 165 (2007) 581.
[46] R.P. Williams, Ph.D. Thesis, University of Newcastle, 1996.

## Glossary of terms

*General terms*

*CV:* Cyclic voltammetry
*EIS:* Electrochemical impedance spectroscopy
*GITT:* Galvanostatic intermittent titration technique
*LSV:* Linear sweep voltammetry
*OCV:* Open-circuit voltage (V or mV)
*Processes 1 and 2:* Individual discharge processes during the overall electrode discharge
*SPECS:* Step potential electrochemical spectroscopy

*Chronoamperometric model terms*

*a:* Spherical particle radius (m or cm)
*A:* Electrochemically active surface area ($\mathrm{m^2\,g^{-1}}$ or $\mathrm{cm^2\,g^{-1}}$)

$C^*$: Bulk concentration (mol $L^{-1}$ or mol $m^{-3}$)
$C_0$: Initial concentration (mol $L^{-1}$ or mol $m^{-3}$)
$C(x, t)$: Spatial and time dependent species concentration
$\Delta C$: Change in species concentration after discharge (mol $L^{-1}$ or mol $m^{-3}$)
$D$: Diffusion coefficient ($m^2\ s^{-1}$ or $cm^2\ s^{-1}$)
$F$: Faraday constant (96,485 C $mol^{-1}$)
$i(t)$: Time-dependent current (A $g^{-1}$ or mA $g^{-1}$)
$i_d(t)$: Diffusion-limited current (A $g^{-1}$ or mA $g^{-1}$)
$n$: Stoichiometric number of electrons transferred
$Q$: Capacity (C $g^{-1}$)
$t$: Time (s)